CORTEX 158 (2023) 127–136

Available online at www.sciencedirect.com

ScienceDirect

Journal homepage: www.elsevier.com/locate/cortex

Research Report

High precision magnetoencephalography reveals increased right-inferior frontal gyrus beta power during response conflict

Pria L. Daniel [a,*], James J. Bonaiuto [b,c], Sven Bestmann [d,e], Adam R. Aron [a] and Simon Little [f]

[a] Department of Psychology, University of California San Diego, CA, USA
[b] Institut des Sciences Cognitives, Marc Jeannerod, CNRS UMR5229, Bron, France
[c] Université Claude Bernard Lyon 1, Université de Lyon, Lyon, France
[d] Wellcome Centre for Human Neuroimaging, UCL Queen Square Institute of Neurology, University College London, London, UK
[e] Department for Clinical and Movement Neuroscience, UCL Queen Square Institute of Neurology, University College London, London, UK
[f] Department of Neurology, University of California San Francisco, CA, USA

ARTICLE INFO

Article history:
Received 24 May 2022
Reviewed 3 July 2022
Revised 14 September 2022
Accepted 10 October 2022
Action editor Sonja Kotz
Published online 26 November 2022

Keywords:
R-IFG beta
Response conflict
Switching
hpMEG
pre-SMA theta

ABSTRACT

Flexibility of behavior and the ability to rapidly switch actions is critical for adaptive living in humans. It is well established that the right-inferior frontal gyrus (R-IFG) is recruited during outright action-stopping, relating to increased beta (12–30 Hz) power. It has also been posited that inhibiting incorrect response tendencies and switching is central to motor flexibility. However, it is not known if the commonly reported R-IFG beta signature of response inhibition in action-stopping is also recruited during response conflict, which would suggest overlapping networks for stopping and switching. In the current study, we analyzed high precision magnetoencephalography (hpMEG) data recorded with multiple within subject recording sessions (trials $n > 10{,}000$) from 8 subjects during different levels of response conflict. We hypothesized that a R-IFG-triggered network for response inhibition is domain general and therefore also involved in mediating response conflict. We tested whether R-IFG showed increased beta power dependent on the level of response conflict. Using event-related spectral perturbations and linear mixed modeling, we found that R-IFG beta power increased for response conflict trials. The R-IFG beta increase was specific to trials with strong response conflict, and increased R-IFG beta power related to less error. This supports a more generalized role for R-IFG beta, beyond simple stopping behavior towards response switching.

* *Corresponding author.*
E-mail addresses: pldaniel@ucsd.edu (P.L. Daniel), james.bonaiuto@isc.cnrs.fr (J.J. Bonaiuto), s.bestmann@ucl.ac.uk (S. Bestmann), adamaron@ucsd.edu (A.R. Aron), Simon.Little@ucsf.edu (S. Little).
https://doi.org/10.1016/j.cortex.2022.10.007

1. Introduction

Sometimes we plan or start to execute an action, but then need to suddenly execute a different action instead. In experiments, this has been called switching, response overriding, or overcoming response conflict; here we use the term response conflict. One notable theory suggests that during motoric response conflict, inhibition of the incorrect response tendency is necessary (see Wiecki & Frank, 2013). This inhibitory control mechanism may be the same as that of outright action-stopping (e.g., Wessel & Aron, 2017; Wessel et al., 2019), although a subsequent response is not required when stopping. However, it remains an open question to what extent response conflict resolution and stopping rely on shared mechanisms of inhibition.

Communication from the right-inferior frontal gyrus (R-IFG) to the STN of the basal ganglia has been implicated in stopping movement (for review, see Aron et al., 2016; Hannah & Aron, 2021). Specifically, previous studies have found increased beta (12–30 Hz) power in R-IFG (Swann et al., 2009; Wagner et al., 2018; Schaum et al., 2021; Sundby et al., 2021) and STN (for review, see Zavala et al., 2015) during successful stopping. The notion that mechanisms of response inhibition are important for overcoming response conflict by inhibiting incorrect response tendencies has been supported by computational models (Wiecki & Frank, 2013) and empirical work (Brittain et al., 2012; Forstmann et al., 2008a, 2008b; Neubert et al., 2010; Wessel et al., 2019). However, scant research has implicated R-IFG in response conflict, despite it being a key node in the putative inhibitory control network. Neubert et al. (2010) found using transcranial magnetic stimulation (TMS) that response conflict increased the inhibitory influence of R-IFG over primary motor (M1) cortical representations of incorrect responses. Using fMRI, Forstmann and colleagues (2008a, 2008b) found that R-IFG activation related to behavioral indices of response inhibition during response conflict, although only for some trials. This suggests that R-IFG may be recruited to inhibit incorrect responses during response conflict, but the limited evidence has not yet been supported by high resolution electrophysiology. Brittain et al. (2012) reported increased STN beta during Stroop conflict, which might suggest that beta-band communication from R-IFG to STN is involved in overcoming response conflict. However, to date there has not been a direct electrophysiological investigation of the role of R-IFG beta during response conflict, which is the primary focus of the current study.

Other cortical regions are thought to facilitate the control of action during conflict as well. Communication from pre-SMA to the STN has been implicated in conflict (for review, see Aron et al., 2016). Medial prefrontal cortex (mPFC), including pre-SMA, has been implicated during response conflict paradigms using neuroimaging (Garavan et al., 2003; Nachev et al., 2005), brain stimulation (Neubert et al., 2010), electrophysiology (Wessel et al., 2019; Zavala et al., 2018), and single-unit recordings (Isoda & Hikosaka, 2007). A common electrophysiological readout during response conflict is increased theta (4–8 Hz) power in mPFC (Wessel et al., 2019; Zavala et al., 2018) – plausibly originating from pre-SMA – and in STN (Zavala et al., 2018). This theta increase has been interpreted as a "pause" of motor output while evidence accumulates to a decision threshold (see Wiecki & Frank, 2013). It is a secondary focus of the current study to attempt to replicate previous findings implicating mPFC theta power during response conflict.

We re-analyzed a head-cast, high precision MEG (hpMEG) dataset with >10,000 trials from a small cohort of healthy controls ($N = 8$) during a random dot kinematogram (RDK) response conflict paradigm (Bonaiuto et al., 2018; Little et al., 2019). We reconstructed source activity in R-IFG, left-IFG (L-IFG; R-IFG control region), and pre-SMA. We then utilized event-related spectral perturbations and linear mixed modeling to evaluate power changes associated with response conflict at the single-trial level, following an imperative cue which could be congruent or incongruent with the preparatory cue. We hypothesized that R-IFG beta is recruited for response inhibition during response conflict, and tested whether R-IFG beta power increased on response conflict trials, particularly strong response conflict. We also evaluated classical mPFC theta activity by testing whether pre-SMA theta power increased on response conflict trials. Lastly, we tested whether changes in R-IFG beta and pre-SMA theta power during response conflict related to motor behavior.

2. Materials and methods

We report how we determined our sample size, all data exclusions (if any), all data inclusion/exclusion criteria, whether inclusion/exclusion criteria were established prior to data analysis, all manipulations, and all measures in the study.

2.1. *Data and code availability*

The analyses presented in this paper were performed on a pre-existing hpMEG dataset, collected with subject-specific head-casts to maximize signal-to-noise ratio (SNR) (see Little et al., 2018). Raw data are available via the Open Science Framework (OSF) at https://osf.io/eu6nx, and via the Open MEG Archive (OMEGA; Niso et al., 2016) at https://doi.org/10.23686/0015896 (register at https://www.mcgill.ca/bic/resources/omega; Niso et al., 2018), and processed data are available via OSF at https://osf.io/hqaw6. The code used to present experimental stimuli is available via Github at https://github.com/jbonaiuto/cued_action_selection. The analyses presented here were performed with custom scripts in MATLAB R2020a and RStudio Version 1.2.5001, which are available via OSF at https://osf.io/hqaw6.

A full description of the original materials and methods can be found in the original description (Bonaiuto et al., 2018). Brief summaries of key features of the initial data collection and processing are included here, along with more detailed information about the methods used that differ from the original techniques. Study procedures and analyses were not pre-registered.

2.2. Response conflict paradigm

Subjects were presented with RDKs that predicted upcoming movement cues and varied in level of coherence (high, medium, low; each 33.3% of trials). The preparatory RDKs were followed by an imperative cue that indicated a left or right button press using the middle or index finger of the right hand, and were either congruent with the preparatory cue (no response conflict; 70% of trials) or incongruent (response conflict; 30% of trials) (Figure 1). We operationally defined low RDK coherence incongruent trials as having a low strength of response conflict, medium RDK coherence incongruent trials as having a medium strength of response conflict, and high RDK coherence incongruent trials as having a high strength of response conflict. On each trial, subjects responded to an imperative cue using either the index or middle finger of their right hand. Between trials, subjects fixated on a central fixation cross (not depicted in Figure 1).

The sample size was determined by that of the original study. Eight subjects completed 1–4 sessions each, for a total of 24 sessions in the dataset. Prior to data visualization and statistical analysis, we excluded trials with a response time (RT) of less than 100 ms, resulting in a total of 10,496 trials included across all subjects (512–2109 trials per subject). Neural signals were analyzed after the imperative cue, before the average RT, to index response conflict. We did not analyze neural signals during the RDK period, as this has been previously reported (Bonaiuto et al., 2018; Little et al., 2019).

2.3. Source inversion

Sensor-level hpMEG data (recorded during the response conflict paradigm) was source inverted using individual subjects' cortical surface meshes to reconstruct activity in R-IFG, L-IFG, and pre-SMA. We analyzed source data from L-IFG as a control region for R-IFG. For source inversion, cortical surface meshes were extracted using FreeSurfer (Fischl, 2012) from multiparameter maps using the proton density (PD) and longitudinal relaxation time (T1) sequences from each subject's structural MRI, as described by Bonaiuto et al. (2018). 3-Dimensional surface plots of each subject's cortical surface mesh were reviewed and subject-specific regions of interest (ROIs) were

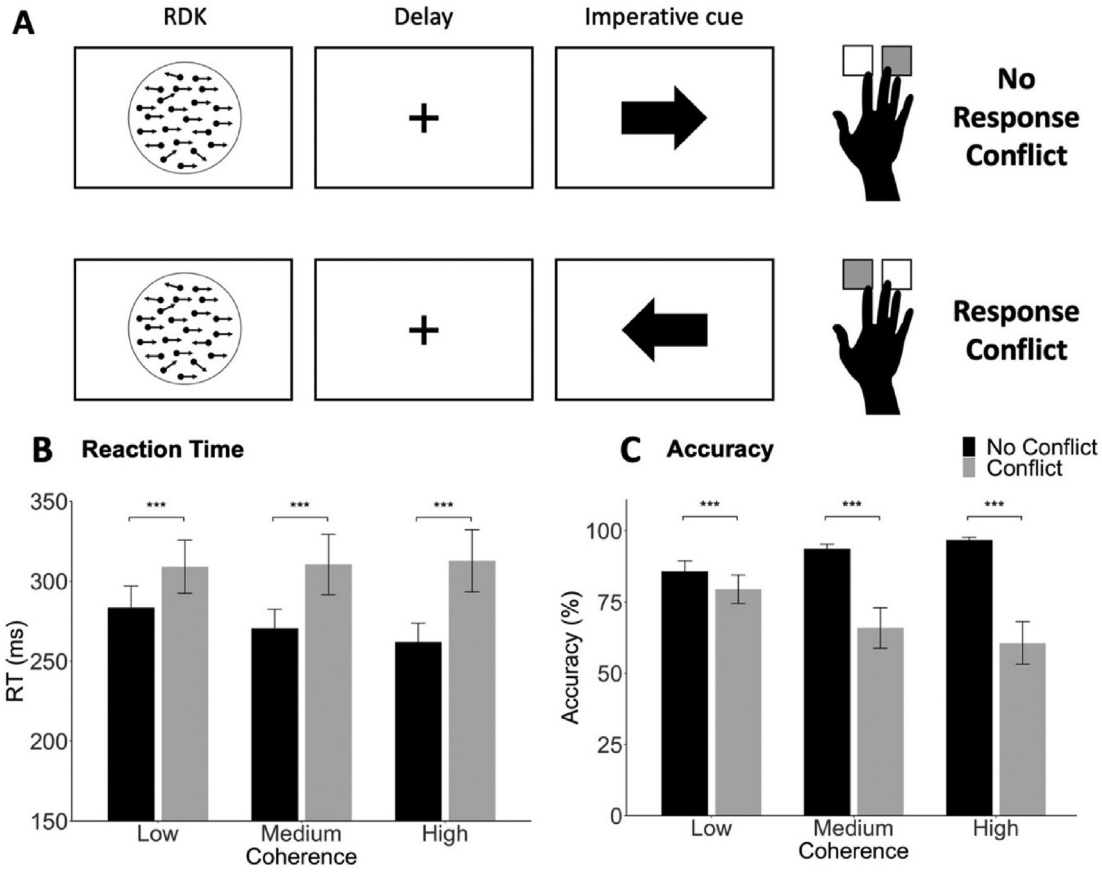

Figure 1 – Response conflict paradigm and behavioral performance. A. On each trial, subjects were shown a random dot kinematogram (RDK) that varied in level of coherence (high, medium, or low), followed by a fixation cross for a delay period. On a majority of trials (70%), the RDK accurately predicted the direction of the imperative cue, resulting in no response conflict (top panel). On a minority of trials (30%), the RDK inaccurately predicted the direction of the imperative cue, resulting in response conflict (bottom panel). Left and right button press responses were made with the index and middle fingers, respectively, of the right hand. B and C. Subjects responded significantly faster (B) and more accurately (C) on trials with no response conflict compared to trials with response conflict. Error bars represent standard error of the mean, at the session level ($N = 24$). ***$p < .0001$.

established using previously defined anatomical landmarks: right and left pars opercularis for R-IFG and L-IFG, respectively (see Levy & Wagner, 2011; Breshears et al., 2019), and right dorsomedial PFC for pre-SMA (see Kim et al., 2010; Neubert et al., 2010; Zhang et al., 2011). Next, we selected a central vertex within each region, and validated our selection using MNI coordinates from meta-analyses on NeuroSynth (Yarkoni et al., 2011). We created localized clusters by selecting all vertices within a 1 mm radial distance across the cortical surface (see Figures 2A and 3A for a visualization of one subject as an example). We then performed source inversion using SPM 12 (http://www.fil.ion.ucl.ac.uk/spm/) and an Empirical Bayesian beamformer, as described by Little et al. (2019), and then selected source activity time series for every vertex in each ROI cluster for further analysis.

2.4. Time-frequency decomposition

We computed time-frequency transforms of the source-level time series using Morlet wavelets (3 cycles at low frequencies, linearly increasing by .5 at higher frequencies), with a range from 4 to 30 Hz (see Jana et al., 2020). We performed time-frequency transforms for the time series for every vertex in each ROI cluster, to obtain a time × frequency × trial × vertex, 4-dimensional matrix of power for each ROI in each session. Then, we averaged across the cluster vertex dimension to create a time × frequency × trial matrix.

2.4.1. Event-related spectral perturbation (ERSP)

For group level visualizations, we computed ERSPs for trials with and without response conflict for each ROI (i.e., R-IFG, L-IFG, pre-SMA). We converted spectral power to decibels (dB) using a 500 ms baseline prior to the RDK presentation (i.e., during fixation) (see Cohen, 2014). We averaged across all sessions that each subject completed (total $N = 24$), and then computed a grand average across subjects ($N = 8$). We subtracted the group average ERSP for trials with no response conflict from the group average ERSP for trials with response conflict to specifically visualize the difference. We plotted these ERSPs with a range from 4 to 30 Hz on the *y*-axis and 0–500 ms relative to the imperative cue on the *x*-axis, with a vertical line at 300 ms denoting average RT (Figure 2). We followed the same procedure for R-IFG ERSPs split by levels of coherence (Figure 3).

2.5. Statistical analyses

To optimize analysis across all trials ($n = 10{,}496$) in this dataset, and model within-subject data as well as small cohort

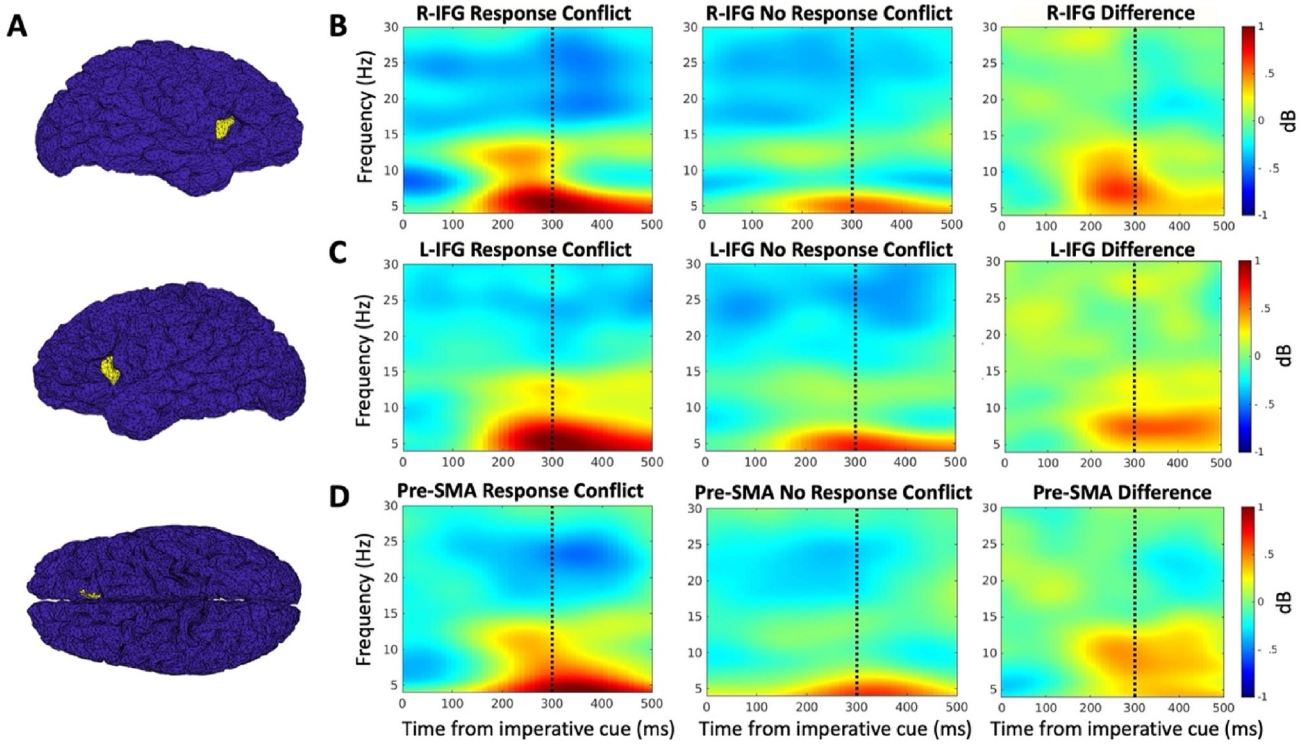

Figure 2 – ERSPs for R-IFG, L-IFG, and pre-SMA. Group-average event-related spectral perturbations (ERSPs) for response conflict trials, no response conflict trials, and their difference. Dashed vertical line at 300 ms denotes average RT. Statistics were performed at the single-trial level; these group-level plots are solely for visualization. A. Example source localization for R-IFG (top), L-IFG (middle), and pre-SMA (bottom) from one subject. B. R-IFG shows increased theta and low beta power prior to the average RT for response conflict trials compared to no response conflict trials. Single-trial analyses revealed significant main effects of response conflict on theta, conventional low beta, and subject-specific low beta power. C. L-IFG shows increased theta power (not beta power) prior to the average RT for response conflict trials compared to no response conflict trials. D. Pre-SMA shows increased theta and low beta power prior to the average RT for response conflict trials compared to no response conflict trials.

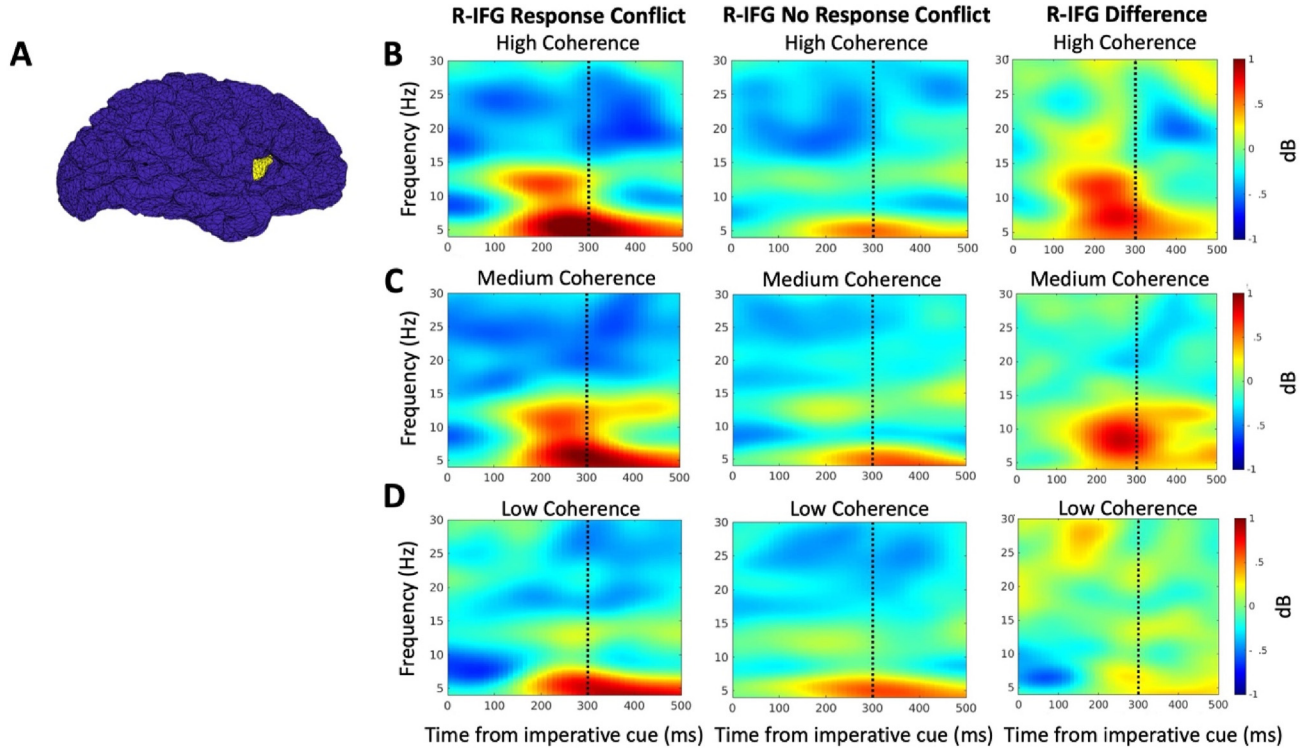

Figure 3 – ERSPs for R-IFG, split by coherence level. Group-average event-related spectral perturbations (ERSPs) for response conflict trials, no response conflict trials, and their difference, by coherence level. Dashed vertical line at 300 ms denotes average RT. Statistics were performed at the single-trial level; these group-level plots are solely for visualization. A. Example source localization for R-IFG from one subject. B-D. R-IFG shows increased low beta and theta power prior to the average RT for response conflict trials compared to no response conflict trials for high coherence (B) and medium coherence (C) trials, and not for low coherence (D) trials. Single-trial analyses revealed a significant interaction between response conflict and coherence on subject-specific low beta power. Pairwise comparisons revealed a significant difference in subject-specific low beta power for response conflict trials compared to no response conflict trials for high coherence trials only, not for medium nor low coherence trials.

between-subject data ($N = 8$), we used a linear mixed modeling framework using R (v3.6.1, R Core Team, 2019) and the lme4 package (v1.1-21, Bates et al., 2015). To compute effect sizes of main effects in our models, we used a formula for Cohen's *d* for mixed effects models (Brysbaert & Stevens, 2018).

2.5.1. *Data preparation for linear mixed modeling*

To prepare the spectral power data for single-trial level statistical analyses, we computed a simple linear baseline subtraction using a 500 ms window prior to the RDK presentation on that trial (see Cohen, 2014; Grandchamp & Delorme, 2011). We a priori (i.e., prior to visualization of the contrast spectrograms) defined time and frequency ranges to average across to obtain single-trial power estimates in our prespecified ROIs. We used 0–300 ms relative to the imperative cue (i.e., time between imperative cue presentation and average RT) as our temporal ROI. We used 4–8 Hz for theta, and subject-specific and conventional partitions of 12–30 Hz for beta (explained in detail in 2.5.1.1). We z-scored each of these single-trial power estimates within-subject and -ROI.

2.5.1.1. Partitioning the beta band. Previous studies have defined beta differently (e.g., Engel & Fries, 2010; Newson & Thiagarajan, 2019; Schmidt et al., 2019). Here we defined 12–20 Hz as 'low beta' and 21–30 Hz as 'high beta'. Previous work has specifically implicated the lower beta band in stopping-related activity (Engel & Fries, 2010; Schmidt et al., 2019; Wagner et al., 2018), so we sought as our primary test an evaluation of whether R-IFG low beta specifically was recruited during response conflict. We used an individualized (peak-centered) frequency band of task-relevant low beta to test our primary hypothesis about R-IFG low beta in response conflict.

We computed average baseline-corrected spectral power (dB) for all trials that the subject completed, and then averaged across our 0–300 ms time window of interest to obtain a single spectral power estimate for each frequency value in the 12–20 Hz range. Then we extracted the value for which low beta power was greatest, and used that as the center of a narrow subject-specific range (peak low beta ±1 Hz). In addition to defining subject-specific low beta, we also used a broader band conventional range of low beta (12–20 Hz) and used the same procedure described here to define subject-specific (peak high beta ±1 Hz) and conventional (21–30 Hz) high beta for secondary comparison. Notably, we saw distinct baseline-corrected low beta peaks separate from the theta band in 7 out of 8 subjects for R-IFG (1 subject appeared to have

an incomplete beta peak). The mean peak low beta value in R-IFG was 13.79 Hz (±1.05 Hz), in L-IFG it was 13.71 Hz (±.93 Hz), and in pre-SMA it was 15.99 Hz (±1.35 Hz).

2.5.2. *Linear mixed models*

All of our models were structured with session nested within subject-specific intercepts as random effects. We used Type III Wald Chi Square tests for our models. We used z-tests, Tukey corrected for multiple comparisons, for pairwise comparisons.

To assess the impact of response conflict and RDK coherence on RT, we used a linear mixed model with RT (log10 transformed) as the dependent variable, and response conflict, RDK coherence, and their interaction as fixed effects. To assess the impact of response conflict and RDK coherence on error, we used a generalized linear mixed model with a binomial distribution, response (0 = incorrect, 1 = correct) as the dependent variable, and response conflict, RDK coherence, and their interaction as fixed effects. To assess the impact of response conflict and RDK coherence on neural activity, we used linear mixed models with z-scored power as the dependent variable, and response conflict, RDK coherence, and their interaction as fixed effects. Lastly, to explore relationships between neural activity and behavior (i.e., RT, error), we used linear mixed models with RT (log10 transformed) as the dependent variable, and z-scored power, response conflict, and their interaction as fixed effects, and generalized linear mixed models with a binomial distribution, response (0 = incorrect, 1 = correct) as the dependent variable, and z-scored power, response conflict, and their interaction as fixed effects.

3. Results

3.1. *Behavioral results*

On average, subjects responded faster and more accurately on trials with no response conflict compared to trials with response conflict (Figure 1). Linear mixed models revealed a significant interaction between response conflict and coherence on log-transformed RT ($X^2(2) = 35.3$, $p < .0001$) and on response accuracy ($X^2(2) = 264.19$, $p < .0001$). Pairwise comparisons revealed significant differences in behavioral performance for trials with no response conflict compared to trials with response conflict. Subjects had significantly longer RTs on trials with response conflict for high ($Z = -17.07$, $p < .0001$), medium ($Z = -14.18$, $p < .0001$) and low ($Z = -8.93$, $p < .0001$) coherence trials, and significantly more errors on trials with response conflict for high ($Z = 26.94$, $p < .0001$), medium ($Z = 20.64$, $p < .0001$), and low ($Z = 4.81$, $p < .0001$) coherence trials.

3.2. *Neural results*

3.2.1. *Increased beta power during response conflict in R-IFG, not L-IFG or pre-SMA*

To test whether there was increased low beta power in R-IFG during response conflict, we analyzed subject-specific and conventional low beta power during response conflict trials compared to no response conflict trials in R-IFG. We also secondarily analyzed subject-specific and conventional high beta for comparison. On average, low beta power in R-IFG was higher during response conflict trials compared to no response conflict trials (Figure 2B). Our linear mixed models revealed a significant main effect of response conflict on subject-specific ($X^2(1) = 16.17$, $p < .0001$; $d = .15$) and conventional ($X^2(1) = 4.25$, $p = .039$; $d = .08$) low beta power in R-IFG. Our linear mixed models revealed no significant main effects of response conflict on conventional nor subject-specific definitions of high beta power in R-IFG.

We then tested the relationship between response conflict and beta power in L-IFG and pre-SMA to test for regional specificity of any beta increases. Although visually, low beta power in pre-SMA also appeared to be slightly higher during response conflict trials compared to no response conflict trials (Figure 2D), our linear mixed models revealed no significant main effects of response conflict on subject-specific nor conventional definitions of low nor high beta power in pre-SMA. Additionally, there was no difference in L-IFG beta power on response conflict trials compared to no response conflict trials (Figure 2C), and our linear mixed models revealed no significant main effects of response conflict on subject-specific nor conventional definitions of low nor high beta power in L-IFG.

3.2.2. *R-IFG beta power increased for stronger response conflict trials*

To test whether the recruitment of R-IFG low beta power during response conflict depended on the strength of the response conflict, we looked at the interaction between response conflict and RDK coherence (operationalized as modulating the strength of response conflict on incongruent trials) on subject-specific and conventional low beta power. On average, low beta power in R-IFG was higher during response conflict trials compared to no response conflict trials for high coherence trials (Figure 3B) and for medium coherence trials (Figure 3C), and not for low coherence trials (Figure 3D). Our linear mixed models revealed a significant interaction between response conflict and coherence on subject-specific low beta power in R-IFG ($X^2(2) = 6.76$, $p = .034$), and not on conventional low beta power. Pairwise comparisons revealed a significant difference in subject-specific R-IFG low beta power for high coherence (i.e., strong) response conflict trials compared to high coherence no response conflict trials ($Z = -4.02$, $p = .0001$), and not for within medium nor low coherence trials.

3.2.3. *Increased theta power during response conflict in pre-SMA, R-IFG, and L-IFG*

To test for previously described theta power increases in mPFC during response conflict, we analyzed pre-SMA theta power during response conflict trials compared to no response conflict trials. We also analyzed theta power in R-IFG and L-IFG to test for regional specificity of any theta increases. Theta power after the presentation of the imperative cue was higher during response conflict trials compared to no response conflict trials in pre-SMA (Figure 2D), R-IFG (Figure 2B), and L-IFG (Figure 2C). Our linear mixed models revealed a trend of a main effect of response conflict on pre-SMA theta power ($X^2(1) = 2.82$, $p = .093$; $d = .06$), a significant main effect of

response conflict on R-IFG theta power ($X^2(1) = 12.07$, $p = <.0001$; $d = .13$), and a trend of a main effect of response conflict on L-IFG theta power ($X^2(1) = 3.16$, $p = .075$; $d = .07$).

3.2.4. *R-IFG and L-IFG theta power increased for stronger response conflict trials*

To test whether the recruitment of theta during response conflict depended on the strength of the response conflict, we also looked at the interaction between response conflict and RDK coherence on theta power in pre-SMA, R-IFG, and L-IFG. Our linear mixed models revealed a significant interaction between response conflict and coherence on theta power in R-IFG ($X^2(2) = 13.13$, $p = .0014$) and in L-IFG ($X^2(2) = 10.44$, $p = .0054$), and not in pre-SMA. Pairwise comparisons revealed a significant difference in R-IFG theta power for high coherence (i.e., strong) response conflict trials compared to high coherence no response conflict trials ($Z = -3.47$, $p = .0005$) and within medium coherence trials ($Z = -2.47$, $p = .014$), and not for within low coherence trials. Pairwise comparisons revealed a trend of a significant difference in L-IFG theta power within high coherence trials ($Z = -1.78$, $p = .076$), a significant difference within medium coherence trials ($Z = -3.92$, $p = .0001$), and no significant difference within low coherence trials.

3.3. *Neural and behavioral results*

3.3.1. *Increased R-IFG beta power relates to less error in responding*

Following the finding of an increase in R-IFG low beta power during response conflict (3.2.1 and 3.2.2), we sought to test whether this increase related to behavior. We found no significant relationships between R-IFG beta and RT. Using generalized linear mixed models with a binomial distribution and response (0 = incorrect, 1 = correct) as the dependent variable, we found a significant interaction between R-IFG beta and response conflict on response accuracy for subject-specific ($X^2(1) = 9.09$, $p = .0026$) and conventional ($X^2(1) = 9.57$, $p = .002$) low beta power in R-IFG. For trials with no response conflict, there was a significant relationship between increased R-IFG beta and less error in responding for subject-specific ($Z = 2.31$, $p = .021$) and conventional ($Z = 2.69$, $p = .0071$) definitions of low beta. For trials with response conflict, there were no significant relationships between R-IFG beta and response accuracy. However, there was a trend for a relationship between increased subject-specific R-IFG low beta and more error in responding for trials with response conflict ($Z = -1.94$, $p = .053$).

3.3.2. *Increased pre-SMA theta power relates to slower responding*

Although we did not find a significant increase in pre-SMA theta power during response conflict ($p = .093$; see 3.2.3), we had a priori predictions about the role of pre-SMA theta power in response conflict, so we conducted exploratory analyses to test the relationship between increased pre-SMA theta and behavior. Using a linear mixed model with log-transformed RT as the dependent variable, we found a significant interaction between pre-SMA theta power and response conflict on RT ($X^2(1) = 4.24$, $p = .039$). For trials with no response conflict, there was a significant relationship between increased pre-SMA theta and longer RTs ($Z = 3.30$, $p = .001$). For trials with response conflict, there was no significant relationship between pre-SMA theta and RT. We found no significant relationships between pre-SMA theta power and response accuracy.

3.3.3. *Increased R-IFG and L-IFG theta power relates to more error in responding*

Lastly, given that we saw increased R-IFG and L-IFG theta power for trials with stronger response conflict (3.2.4), we sought to test whether this increase related to behavior. We found no significant relationships between R-IFG or L-IFG theta and RT. Using generalized linear mixed models with a binomial distribution and response (0 = incorrect, 1 = correct) as the dependent variable, we found a significant interaction between R-IFG theta and response conflict on response accuracy ($X^2(1) = 6.23$, $p = .012$). For trials with response conflict, there was a significant relationship between increased R-IFG theta and more error in responding ($Z = -4.51$, $p < .0001$), and no significant relationship for trials with no response conflict. We also found a significant main effect of L-IFG theta on response accuracy ($X^2(1) = 4.77$, $p = .029$, $d = .06$), where increased L-IFG theta related to more error in responding for trials with response conflict ($Z = -2.18$, $p = .03$) and trials without response conflict ($Z = -2.34$, $p = .019$).

4. Discussion

We found support for our theoretically driven, a priori hypothesis about the recruitment of R-IFG beta during response conflict. We hypothesized that response switching is a generalized form of stopping and therefore would recruit the previously defined R-IFG beta-triggered inhibitory control network during response conflict. A small number of studies have directly implicated R-IFG activity using response conflict paradigms (Forstmann et al., 2008a, 2008b; Neubert et al., 2010). However, these studies have not used high spatial and temporal resolution neuroimaging as afforded by head-cast hpMEG. Increased R-IFG beta activity is usually simply interpreted as a marker of successful response inhibition in the stop-signal task (Schaum et al., 2021; Swann et al., 2009; Wagner et al., 2018). It has been proposed that beta-band communication from R-IFG to STN to M1 stops motor output (see Aron et al., 2016; Hannah et al., 2021), which is supported by increased STN beta power during successful stopping (Bastin et al., 2014; Ray et al., 2012). One notable computational framework (Wiecki & Frank, 2013) posits that mechanisms of response inhibition are important to overcome response conflict, such that one needs to inhibit an incorrect prepotent response tendency in order to execute the correct response in a conflict scenario. This idea has been supported by various empirical studies (Brittain et al., 2012; Forstmann et al., 2008a, 2008b; Neubert et al., 2010; Wessel et al., 2019), but until now, there has been no direct empirical evidence to support R-IFG beta (i.e., a marker of response inhibition in the action-stopping literature) during response conflict and action switching.

Importantly, we found here that low beta power in R-IFG was significantly increased on trials with response conflict

compared to trials without response conflict. Previous electrophysiological work has shown that the right prefrontal beta marker of successful response inhibition during stopping occurs in the lower part of the beta band (Engel & Fries, 2010; Schmidt et al., 2019; Wagner et al., 2018), and our results regarding the significance of low beta, not high beta, are consistent with this. Notably, we did not see any significant increases in beta power in L-IFG. This is a strong control region for R-IFG because it is an anatomically matched prefrontal region, but one that is not hypothesized to be a node in the putative inhibitory control network. Another compelling component of this result is that this R-IFG low beta increase during response conflict was specific to trials with stronger response conflict. R-IFG beta power significantly increased for high coherence response conflict trials, increased for medium coherence response conflict trials but was not significant, and did not increase for low coherence response conflict trials. We predicted that punctate response inhibition (plausibly via R-IFG beta power) might be necessary when the incorrect response tendency is most prepotent (i.e., during strong conflict trials), and our results support this idea. Supporting this further, we found a significant relationship between R-IFG low beta power and less error in responding. This analysis looks at endogenous trial-by-trial fluctuations in beta within response conflict or no response conflict trials. This relationship was only significant on trials with no response conflict. Taken together, these results support a potential inhibitory control role for R-IFG beta in overcoming response conflict, though the trial-by-trial relationship between R-IFG beta and behavioral performance should continue to be investigated in future studies.

Additionally, in line with previous literature we secondarily predicted that pre-SMA theta power would increase during response conflict. We hypothesized that pre-SMA is a central region for overcoming response conflict, supported by findings in humans and non-human primates (Garavan et al., 2003; Isoda & Hikosaka, 2007; Nachev et al., 2005; Neubert et al., 2010). Electrophysiology studies have shown increased mPFC theta in response conflict paradigms (Wessel et al., 2019; Zavala et al., 2018), which plausibly originates from pre-SMA. However, in our current study, we found that after the imperative cue and prior to the average RT, there was only a trend of an increase in pre-SMA theta power during trials with response conflict, but this did not reach significance. In an exploratory analysis, we found a significant relationship between pre-SMA theta power and slower RTs, which aligns with a framework implicating pre-SMA theta in pausing motor output (see Wiecki & Frank, 2013; Aron et al., 2016). However, this relationship was only significant for trials with no response conflict, which may reflect possible differences between pre-SMA coding of classic sensorimotor conflict versus response conflict or potentially ceiling effects on high conflict trials. Additionally, in the current study we found that theta power in R-IFG and L-IFG significantly increased for stronger (i.e., medium or high coherence) conflict trials. This indicates a lack of regional specificity for theta activity which we did not initially predict. This could reflect the high SNR in our data, and could suggest a broader recruitment of cortical theta during response conflict than has previously been reported. In exploring the potential role of this recruitment of IFG theta in response conflict, we found that increased theta power in R-IFG and L-IFG significantly related to more error in responding on trials with response conflict. Overall, it is interesting to note that the theta effect appeared less localized to medial PFC than suggested by previous literature and in comparison to the beta effect. Future work could investigate this explicitly, as well as interactions between the theta and beta signals and their behavioral outcomes (notably their dissociable relationships with RT versus accuracy shown here) under different types of conflict.

Some limitations of our study merit explicit discussion. We analyzed hpMEG data collected from a small cohort of 8 subjects. Although this is a relatively low number of human subjects, the hpMEG data was recorded across multiple sessions per subject affording high numbers of trials per subject (total trials $n = 10{,}496$) and had high SNR. Subject-specific head-cast hpMEG allows for low within-subject movement, which supports data analysis that models both within- and between-subject variance (rather than averaging within-subject), and allows for inferences regarding within-subject trial-by-trial neural correlates. This approach was also supported by strong a priori hypotheses that were directly tested here. A possible limitation of the paradigm is that subjects always responded to the imperative cue with their right hand. Therefore, it is possible (albeit unlikely) that this resulted in a lateralization of the low beta increase during response conflict. However, if lateralization of motor responses caused lateralization in neural responses, we would expect these to be contralateral (i.e., L-IFG for right hand); the opposite is found here. Additionally, the main finding in which we report a difference across trial types (i.e., response conflict versus no response conflict, mediated by coherence), cannot be explained by hand laterality. Consequently, we propose that the lateralization of our R-IFG findings is unlikely to be strongly attributable to response execution being restricted to the right hand.

In exploring relationships between trial-by-trial fluctuations in neural activity and behavioral performance on the response conflict task, we found a significant relationship between R-IFG low beta power and less error in responding. However, this relationship was only significant for trials without response conflict, and not significant for trials with response conflict. Notably, the generalized linear mixed model that we used for this analysis did not include coherence as a fixed effect. This is because models with coherence as a fixed effect interaction term included did not converge, plausibly because there were so few errors made in the paradigm. We saw in our main neural analysis a significant interaction between response conflict and coherence on neural activity, so it is possible that not being able to include this in our behavioral analysis restricted our ability to detect the complete relationship between R-IFG beta and performance for trials with response conflict. Additionally, a ceiling effect for R-IFG beta activity on trials with response conflict may have impacted our analysis. Future work with other response conflict paradigms, including those that induce higher error rates, can further probe the relationship between R-IFG beta and behavior.

Lastly, we estimated the effect size of the main effects in our mixed models using a formula for Cohen's *d* (Brysbaert &

Stevens, 2018). Notably, few papers report effect sizes in source-localized time-frequency M/EEG analyses on within-subject cognitive electrophysiology using trial-by-trial analyses (e.g., Larson & Carbine, 2017; Tinga et al., 2019). A recent systematic review of source M/EEG data reported ~55% Hedges' *g* values (interpreted similarly to Cohen's d) less than .3 (i.e., small by convention), with ~76% less than .5 (i.e., small-medium by convention) (Dharan et al., 2021). This suggests that our effect size estimates may be comparable to other studies using time-frequency transforms of source-level electrophysiology, but awaits further reporting of future effect size estimates in comparable studies for complete contextualization.

5. Conclusions

In conclusion, we analyzed hpMEG data with high spatial and temporal resolution recorded during a response conflict paradigm, and found support for a theoretically driven hypothesis about the recruitment of R-IFG beta during response conflict. In a novel result, we showed that R-IFG low beta power was significantly increased for response conflict trials, specifically strong response conflict trials which plausibly require mechanisms of punctate response inhibition for correct responding. We found a significant trial-by-trial relationship between R-IFG beta power and less error in responding, although this was only significant for trials with no response conflict. Future work using methods such as TMS or neurofeedback can further establish the causal role of R-IFG beta power in response conflict resolution. Overall, our results support R-IFG beta as a neural mechanism of overcoming response conflict, in addition to action-stopping. This broadens the role for R-IFG beta as a domain general inhibitory control signal, which may have clinical implications for populations with inhibitory control deficits.

Credit Author Statement

Pria L. Daniel: Conceptualization, Formal analysis, Visualization, Writing - Original Draft; **James Bonaiuto**: Investigation, Funding acquisition, Software, Resources, Writing - Review & Editing; **Sven Bestmann**: Resources, Funding acquisition, Writing - Review & Editing; **Adam R. Aron**: Conceptualization, Funding acquisition, Writing - Review & Editing, Supervision; **Simon Little**: Conceptualization, Funding acquisition, Investigation, Resources, Writing - Review & Editing, Supervision.

Open Practices

The study in this article earned Protected Access, Open Data and Open Materials badges for transparent practices. Materials and data for the study are available at https://osf.io/hqaw6.

Declarations of competing interest

None.

Data availability

All research data are available at https://osf.io/hqaw6

Acknowledgments

This work was supported by the Wellcome Trust [105804/Z/14/Z, 203147/Z/16/Z]; the Biotechnology and Biological Sciences Research Council [BB/M00965/1]; the National Institutes of Health [DA026452, NS106822, K23NS120037]; and the European Research Council under the European Union's Horizon 2020 research and innovation programme [ERC-CoG 864550]. We also acknowledge Dr Philip Starr for his anatomical expertise in localizing R- and L-IFG regions, Dr Vignesh Muralidharan for support in writing scripts, Dr Fei Jiang for advice on linear mixed models, and Dr Gareth Barnes for supervising the initial data collection.

REFERENCES

Aron, A. R., Herz, D. M., Brown, P., Forstmann, B. U., & Zaghloul, K. (2016). Frontosubthalamic circuits for control of action and cognition. *Journal of Neuroscience, 36*, 11489–11495. https://doi.org/10.1523/JNEUROSCI.2348-16.2016

Bastin, J., Polosan, M., Benis, D., Goetz, L., Bhattacharjee, M., Piallat, B., Krainik, A., Bougerol, T., Chabardes, S., & David, O. (2014). Inhibitory control and error monitoring by human subthalamic neurons. *Translational Psychiatry, 4*, Article e439. https://doi.org/10.1038/tp.2014.73

Bates, D., Mächler, M., Bolker, B., & Walker, S. (2015). Fitting linear mixed-effects models using lme4. *Journal of Statistical Software, 67*, 1–48. https://doi.org/10.18637/jss.v067.i01

Bonaiuto, J. J., Meyer, S. S., Little, S., Rossiter, H., Callaghan, M. F., Dick, F., Barnes, G. R., & Bestmann, S. (2018). Lamina-specific cortical dynamics in human visual and sensorimotor cortices. *eLife, 7*, Article e33977. https://doi.org/10.7554/eLife.33977

Breshears, J. D., Southwell, D. G., & Chang, E. F. (2019). Inhibition of manual movements at speech arrest sites in the posterior inferior frontal lobe. *Neurosurgery, 85*, E496–E501. https://doi.org/10.1093/neuros/nyy592

Brittain, J. S., Watkins, K. E., Joundi, R. A., Ray, N. J., Holland, P., Green, A. L., Aziz, T. Z., & Jenkinson, N. (2012). A role for the subthalamic nucleus in response inhibition during conflict. *Journal of Neuroscience, 32*, 13396–13401. https://doi.org/10.1523/JNEUROSCI.2259-12.2012

Brysbaert, M., & Stevens, M. (2018). Power analysis and effect size in mixed effects models: A tutorial. *Journal of Cognition, 1*, 1–20. https://doi.org/10.5334/joc.10

Cohen, M. X. (2014). *Analyzing neural time series data: Theory and practice*. MIT Press.

Dharan, A. L., Bowden, S. C., Lai, A., Peterson, A. D. H., Cheung, M. W., Woldman, W., & D'Souza, W. J. (2021). Source data from a systematic review and meta-analysis of EEG and MEG studies investigating functional connectivity in idiopathic generalized epilepsy. *Data in Brief, 39*, 107665. https://doi.org/10.1016/j.dib.2021.107665

Engel, A. K., & Fries, P. (2010). Beta-band oscillations – signaling the status quo? *Current Opinion in Neurobiology, 20*, 156–165. https://doi.org/10.1016/j.conb.2010.02.015

Fischl, B. (2012). FreeSurfer. *NeuroImage, 62*, 774–781. https://doi.org/10.1016/j.neuroimage.2012.01.021

Forstmann, B. U., Jahfari, S., Scholte, H. S., Wolfensteller, U., van den Wildenberg, W. P. M., & Ridderinkhof, K. R. (2008a).

Function and structure of the right inferior frontal cortex predict individual differences in response inhibition: A model-based approach. *Journal of Neuroscience, 28*, 9790–9796. https://doi.org/10.1523/JNEUROSCI.1465-08.2008

Forstmann, B. U., van den Wildenberg, W. P. M., & Ridderinkhof, K. R. (2008b). Neural mechanisms, temporal dynamics, and individual differences in interference control. *Journal of Cognitive Neuroscience, 20*, 1854–1865. https://doi.org/10.1162/jocn.2008.20122

Garavan, H., Ross, T. J., Kaufman, J., & Stein, E. A. (2003). A midline dissociation between error-processing and response-conflict monitoring. *Neuroimage, 20*, 1132–1139. https://doi.org/10.1016/S1053-8119(03)00334-3

Grandchamp, R., & Delorme, A. (2011). Single-trial normalization for event-related spectral decomposition reduces sensitivity to noisy trials. *Frontiers in Psychology, 2*, 236. https://doi.org/10.3389/fpsyg.2011.00236

Hannah, R., & Aron, A. R. (2021). Towards real-world generalizability of a circuit for action-stopping. *Nature Reviews Neuroscience, 22*, 538–552. https://doi.org/10.1038/s41583-021-00485-1

Isoda, M., & Hikosaka, O. (2007). Switching from automatic to controlled action by monkey medial frontal cortex. *Nature Neuroscience, 10*, 240–248. https://doi.org/10.1038/nn1830

Jana, S., Hannah, R., Muralidharan, V., & Aron, A. R. (2020). Temporal cascade of frontal, motor and muscle processes underlying human action-stopping. *eLife, 9*, Article e50371. https://doi.org/10.7554/eLife.50371

Kim, J. H., Lee, J. M., Jo, H. J., Kim, S. H., Lee, J. H., Kim, S. T., Seo, S. W., Cox, R. W., Na, D. J., Kim, S. I., & Saad, Z. S. (2010). Defining functional SMA and pre-SMA subregions in human MFC using resting state fMRI: Functional connectivity-based parcellation method. *Neuroimage, 49*, 2375–2386. https://doi.org/10.1016/j.neuroimage.2009.10.1016

Larson, M. J., & Carbine, K. A. (2017). Sample size calculations in human electrophysiology (EEG and ERP) studies: A systematic review and recommendations for increased rigor. *International Journal of Psychophysiology, 111*, 33–41. https://doi.org/10.1016/j.ijpsycho.2016.06.015

Levy, B. J., & Wagner, A. D. (2011). Cognitive control and right ventrolateral prefrontal cortex: Reflexive reorienting, motor inhibition, and action updating. *Annals of the New York Academy of Sciences, 1224*, 40–62. https://doi.org/10.1111/j.1749-6632.2011.05958.x

Little, S., Bonaiuto, J., Barnes, G., & Bestmann, S. (2019). Human motor cortical beta bursts relate to movement planning and response errors. *PLoS Biology, 17*, Article e3000479. https://doi.org/10.1371/journal.pbio.3000479

Little, S., Bonaiuto, J., Meyer, S. S., Lopez, J., Bestmann, S., & Barnes, G. (2018). Quantifying the performance of MEG source reconstruction using resting state data. *NeuroImage, 181*, 453–460. https://doi.org/10.1016/j.neuroimage.2018/07.030

Nachev, P., Rees, G., Parton, A., Kennard, C., & Husain, M. (2005). Volition and conflict in human medial frontal cortex. *Current Biology, 15*, 122–128. https://doi.org/10.1016/j.cub.2005.01.006

Neubert, F. X., Mars, R. B., Buch, E. R., Olivier, E., & Rushworth, M. F. (2010). Cortical and subcortical interactions during action reprogramming and their related white matter pathways. *Proceedings of the National Academy of Sciences of the United States of America, 107*, 13240–13245. https://doi.org/10.1073/pnas.1000674107

Newson, J. J., & Thiagarajan, T. C. (2019). EEG frequency bands in psychiatric disorders: A review of resting state studies. *Frontiers in Human Neuroscience, 12*, 521. https://doi.org/10.3389/fnhum.2018.00521

Niso, G., Gorgolewski, K. J., Bock, E., Brooks, T. L., Flandin, G., Gramfort, A., Henson, R. N., Jas, M., Litvak, V., Moreau, J. T., Oostenveld, R., Schoffelen, J.-M., Tadel, F., Wexler, J., & Baillet, S. (2018). MEG-BIDS, the brain imaging data structure extended to magnetoencephalography. *Scientific Data, 5*, Article 180110. https://doi.org/10.1038/sdata.2018.110

Niso, G., Rogers, C., Moreau, J. T., Chen, L. Y., Madjar, C., Das, S., Bock, E., Tadel, F., Evans, A. C., Jolicoeur, P., & Baillet, S. (2016). OMEGA: The Open MEG Archive. *Neuroimage, 124*, 1182–1187. https://doi.org/10.1016/j.neuroimage.2015.04.028

R Core Team. (2019). *R: A language environment for statistical computing*. Vienna: R Foundation for Statistical Computing.

Ray, N. J., Brittain, J. S., Holland, P., Joundi, R. A., Stein, J. F., Aziz, T. Z., & Jenkinson, N. (2012). The role of the subthalamic nucleus in response inhibition: Evidence from local field potential recordings in the human subthalamic nucleus. *Neuroimage, 60*, 271–278. https://doi.org/10.1016/j.neuroimage.2011.12.035

Schaum, M., Pinzuti, E., Sebastian, A., Lieb, K., Fries, P., Mobascher, A., Jung, P., Wibral, M., & Tüscher, O. (2021). Right inferior frontal gyrus implements motor inhibitory control via beta-band oscillations in humans. *eLife, 10*, Article e61679. https://doi.org/10.7554/eLife.61679

Schmidt, R., Herrojo Ruiz, M., Kilavik, B. E., Lundqvist, M., Starr, P. A., & Aron, A. R. (2019). Beta oscillations in working memory, executive control of movement and thought, and sensorimotor function. *Journal of Neuroscience, 39*, 8231–8238. https://doi.org/10.1523/JNEUROSCI.1163-19.2019

Sundby, K. K., Jana, S., & Aron, A. R. (2021). Double-blind disruption of right inferior frontal cortex with TMS reduces right frontal beta power for action stopping. *Journal of Neurophysiology, 125*, 140–153. https://doi.org/10.1152/jn.00459.2020

Swann, N., Tandon, N., Canolty, R., Ellmore, T. M., McEvoy, L. K., Dreyer, S., DiSano, M., & Aron, A. R. (2009). Intracranial EEG reveals a time- and frequency-specific role for the inferior frontal gyrus and primary motor cortex in stopping initiated responses. *Journal of Neuroscience, 29*, 12675–12685. https://doi.org/10.1523/JNEUROSCI.3359-09.2009

Tinga, A. M., de Back, T. T., & Louwerse, M. M. (2019). Non-invasive neurophysiological measures of learning: A meta-analysis. *Neuroscience and Biobehavioral Reviews, 99*, 59–89. https://doi.org/10.1016/j.neubiorev.2019.02.001

Wagner, J., Wessel, J. R., Ghahremani, A., & Aron, A. R. (2018). Establishing a right frontal beta signature for stopping action in scalp EEG: Implications for testing inhibitory control in other task contexts. *Journal of Cognitive Neuroscience, 30*, 107–118. https://doi.org/10.1162/jocn_a_01183

Wessel, J. R., & Aron, A. R. (2017). On the globality of motor suppression: Unexpected events and their influence on behavior and cognition. *Neuron, 93*, 259–280. https://doi.org/10.1016/j.neuron.2016.12.013

Wessel, J. R., Waller, D. A., & Greenlee, J. D. W. (2019). Non-selective inhibition of inappropriate motor-tendencies during response-conflict by a fronto-subthalamic mechanism. *eLife, 8*, Article e42959. https://doi.org/10.7554/eLife.42959

Wiecki, T. V., & Frank, M. J. (2013). A computational model of inhibitory control in frontal cortex and basal ganglia. *Psychological Review, 120*, 329–355. https://doi.org/10.1037/a0031542

Yarkoni, T., Poldrack, R. A., Nichols, T. E., Van Essen, D. C., & Wager, T. D. (2011). Large-scale automated synthesis of human functional neuroimaging data. *Nature Methods, 8*, 665–670. https://doi.org/10.1038/nmeth.1635

Zavala, B., Jang, A., Trotta, M., Lungu, C. I., Brown, P., & Zaghloul, K. A. (2018). Cognitive control involves theta power within trials and beta power across trials in the prefrontal-subthalamic network. *Brain, 141*, 3361–3376. https://doi.org/10.1093/brain/awy266

Zavala, B., Zaghloul, K., & Brown, P. (2015). The subthalamic nucleus, oscillations, and conflict. *Movement Disorders, 30*, 328–338. https://doi.org/10.1002/mds.26072

Zhang, S., Ide, J. S., & Li, C. S. (2011). Resting-state functional connectivity of the medial superior frontal cortex. *Cerebral Cortex, 22*, 99–111. https://doi.org/10.1093/cercor/bhr088